

Redox Potential Heterogeneity in Fixed-Bed Electrodes Leads to Microbial Stratification and Inhomogeneous Performance

Jose Rodrigo Quejigo^{+, [a]} Benjamin Korth^{+, [a]} Anne Kuchenbuch,^[a] and Falk Harnisch^{*[a]}

Bed electrodes provide high electrode area-to-volume ratios represent a promising configuration for transferring bioelectrochemical systems close to industrial applications. Nevertheless, the intrinsic electrical resistance leads to poor polarization behavior. Therefore, the distribution of *Geobacter* spp. and their electrochemical performance within exemplary fixed-bed electrodes are investigated. A minimally invasive sampling system allows characterization of granules from different spatial locations of bed electrodes. Cyclic voltammetry of single

granules ($n=63$) demonstrates that the major share of electroactivity (134.3 mA L^{-1}) is achieved by approximately 10% of the bed volume, specifically that being close to the current collector. Nevertheless, analysis of the microbial community reveals that *Geobacter* spp. dominated all sampled granules. These findings clearly demonstrate the need for engineered bed electrodes to improve electron exchange between microorganisms and granules.

Introduction

During the last decade, microbial electrochemical technologies (MET) have become a promising platform to tackle challenges in environmental and industrial biotechnology.^[1] Primary MET are based on the extracellular electron transfer (EET) between electrochemically active microorganisms (EAM) and electrodes.^[2] This EAM-electrode interaction is realized within reactors termed bioelectrochemical systems (BES).

For optimizing the overall BES performance, several aspects have been studied, e.g., fundamentals of biofilm conductivity, and engineered including microbiomes, materials, and reactor architecture.^[3–5] One central aspect for boosting the performance of BES is the design and engineering of electrodes.^[6] Thereby, the general aim is an increased available surface area for EAM at lowest costs and with materials and designs that can be easily upscaled. In this line, a plethora of new electrode designs and materials have been proposed including 3D structures like felts and foams.^[7] Bed electrodes for BES (bed-BES), i.e., 3D electrodes being composed of conductive granules, are promising as they represent a cost effective approach to provide high electrode area-to-volume ratios. BedBES have been used numerous times for different

applications.^[8,9] In terms of operation, fixed-bed electrodes (i.e., static bed of particles) and fluidized bed electrodes (i.e., particles are moved, e.g., by pumping) have to be distinguished.^[9] For bedBES, several carbon-based materials have been utilized including granular activated carbon,^[10,11] graphite granules,^[12,13] and coke.^[14] Furthermore, biochar became of relevance for upscaling as it is a low-cost material with good biocompatibility, chemical stability, and high electrical conductivity.^[15,16] The typical porous structure of all these materials increase their interphase with EAM.^[17]

At the same time, bed electrodes exhibit an increased electrical resistance in comparison to monolithic electrodes (i.e., electrodes formed by a single piece of conductive material) that may hamper their applicability. The reasons for the increased electrical resistance can be summarized as follows: i) In bedBES, the limited physical contact among granules results in low conductivity within the bed. Consequently, the polarization behavior of bed electrodes is poor and potential gradients are likely formed.^[18,19] ii) This phenomenon is reinforced by the porous nature of the conductive materials. Therefore, the electrochemical potential can be assumed to be not identical for all granules and at all sites of a single granule.^[9] iii) Furthermore, the current collector (CC), a necessary element for electrically connecting the assortment of granules, contributes to the resistance. CC are electrochemically inert but electrically conductive materials embedded in the bed electrode. Thus the CC provides an electrical connection between granular bed and external circuit. Sticks, rods, and meshes of graphite,^[12,20] carbon,^[21] titanium,^[22,23] and stainless steel^[24] are commonly used as CC. Traditionally for bedBES, a monolithic rod-shaped CC is embedded, and thereby it is only partially crossing the vertical and horizontal axes of the bed.^[20,21] Rarely, the contact has been established by using graphite plates^[11] or titanium meshes^[22,25] building a transect of the entire axis of the bed electrode and thus providing electrical connection in two

[a] Dr. J. R. Quejigo,⁺ Dr. B. Korth,⁺ A. Kuchenbuch, Prof. F. Harnisch
Department of Environmental Microbiology
Helmholtz Centre for Environmental Research GmbH – UFZ
Permoser Str. 15, 04318 Leipzig (Germany)
E-mail: falk.harnisch@ufz.de

[†] These authors contributed equally to this work.

Supporting information for this article is available on the WWW under <https://doi.org/10.1002/cssc.202002611>

© 2021 The Authors. ChemSusChem published by Wiley-VCH GmbH. This is an open access article under the terms of the Creative Commons Attribution Non-Commercial License, which permits use, distribution and reproduction in any medium, provided the original work is properly cited and is not used for commercial purposes.

dimensions. However, it can be assumed that the connection of CC and granules as well as between individual granules is not as stable as for monolithic electrodes, and therefore the electrochemical potential is not as homogeneous. In summary, this intrinsic electrical resistance of bedBES entails technical drawbacks leading to energy losses as well as analytical limitations. For instance, dynamic electrochemical techniques, e.g., cyclic voltammetry (CV), cannot be straightforwardly applied. Consequently, thermodynamic information on microbial electrochemical reactions in fixed bedBES are insufficient.^[26] Recently, we have introduced a new tool – the e-Clamp – that allowed the CV analysis of single granules derived from a fixed bedBES.^[27]

Although fixed bedBES represent a putative redox stratified environment,^[9] their microbial ecology is sparsely investigated. In contrast, EAM and related microbiomes at monolithic electrodes are well studied.^[28,29] The redox potential is a key variable to shape microbial composition and microbial physiology including thermodynamics and kinetics of EAM.^[30–36] For instance, the two model EAM, *Shewanella oneidensis* MR-1^[37] and *Geobacter sulfurreducens*,^[38,39] utilize different EET pathways depending on the anode potential. Furthermore, *S. oneidensis* possesses sensor molecules for regulating catabolic pathways depending on electrode potential.^[40] When complex microbiomes are cultivated in bedBES, the electrode potential acts as an evolutionary pressure for the microbial community. Consequently, different ecological niches could occur within bedBES being characterized by different potentials due to the unequal potential distribution caused by poor polarization behavior of granular beds.^[9] In this respect, fixed bedBES can be considered as technical habitats being closer to nature than monolithic electrodes as redox stratification naturally occurs in the environment.^[41] Thus, bedBES represent adequate technical environments for studying ecological strategies of EAM and the evolution of versatile metabolic abilities in redox-stratified ecosystems.^[42]

However, the characterization of fixed bedBES in terms of redox stratification and microbial ecology is still scarce. In this article, a systematic spatial electrochemical and genetic investigation of fixed bed anodes is performed. Thereby, the fixed bedBES were inoculated with secondary *Geobacter* spp. enrichment biofilm cultivated in a two-chamber reactor (*Geobacter* abundance $\approx 90\%$) representing a model system for EAM and thus serving as an ideal benchmark.^[43,44] The designed reactor allowed minimally invasive sampling of granules from different zones of the bed anode during operation. The single granules were electrochemically characterized using the e-Clamp and a microbial community structure analysis was performed. Thereby, the influence of potential distribution and poor polarization behavior of granules on spatial *Geobacter* spp. colonization and its electrochemical performance are demonstrated. As a consequence thereof, the need for customized engineering of fixed bedBES is illustrated.

Results and Discussion

Operation and performance of bedBES

Two fixed bed bioelectrochemical systems (bedBES) were operated for 45 d in batch and 15 d in continuous mode (see Figure 1 for bedBES1 and Figure S1 in the Supporting Information for bedBES2). Both reactors showed a stable total charge production of $7.7 \pm 0.9 \text{ kCL}^{-1}$ (bedBES1) and $7.4 \pm 0.7 \text{ kCL}^{-1}$ (bedBES2) per batch cycle regarding bed anode volume. The maximum volumetric current densities (i_{max} , normalized to bed anode volume) during batch cycles varied from 86.2 to 117.2 mA L^{-1} in bedBES1 and from 55.2 to 134.3 mA L^{-1} in bedBES2. After 45 d, reactor operation was changed to continuous mode, i.e., continuous media replacement with HRT of $1.0 \pm 0.1 \text{ d}$. In this second experimental phase, the total charge production was $4.6 \text{ kCd}^{-1} \text{ L}^{-1}$ and $3.8 \text{ kCd}^{-1} \text{ L}^{-1}$ for bedBES1 and bedBES2, respectively, and increased to $7.2 \text{ kCd}^{-1} \text{ L}^{-1}$ and $5.0 \text{ kCd}^{-1} \text{ L}^{-1}$ when acetate concentration was increased from 10 mM to 20 mM. Thereby, i_{max} of bedBES1 were 53.6 mA L^{-1} and 89.3 mA L^{-1} for acetate concentrations of 10 mM and 20 mM, respectively (Figure 1). In contrast, bedBES2 showed lower and unstable i_{max} under both acetate concentrations (Figure S1). For unknown reasons, both reactors experienced a decrease in current production at day 58. Eventually, the limit of three-dimensionality was reached around this moment.^[7,45] Therefore, the formed biomass at the granules started to hinder mass transfer processes (i.e., supply of acetate to EAM and removal of counter ions from biofilm towards liquid) at key positions within the 3D network, i.e., between the granules or in granule pores. Thus, mass transfer became rate limiting leading to a decline of the overall performance.^[46,47] Furthermore, the current decrease could be related to a minuscule movement of the bed (e.g., due to collapsing of voids within the bed caused by sampling of granules) leading to the loss of electrical contact between granules and CC indicating a poor polarization behavior of granular electrode beds (see below).

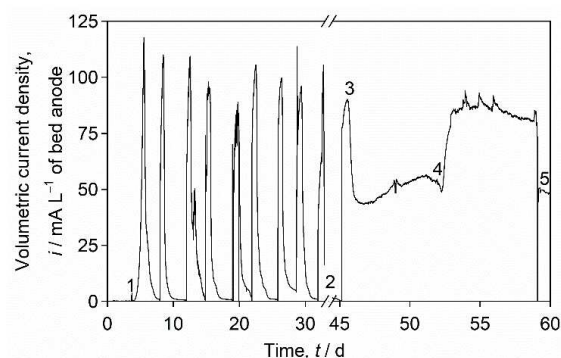


Figure 1. Chronoamperogram of bedBES1 polarized at +200 mV: 1) Inoculation with secondary *Geobacter* spp. enrichment biofilm; 2) granular sampling during batch operation; 3) change in reactor operation from batch to continuous mode; 4) acetate concentration increase from 10 mM to 20 mM; 5) granular sampling during continuous operation (see Figure S1 for bedBES2).

Before inoculation with secondary *Geobacter* spp. enrichment biofilm, no current was registered, but acetate was already removed by approximately 10% (Table S2). This might be assigned to adsorption of acetate at granules and the prevalence of microbial processes as the reactors were not rigorously sterilized before the start of the experiment.

During continuous operation, total acetate removal was achieved for both bedBES with 10 mM acetate. After doubling the acetate concentration to 20 mM, acetate removal decreased slightly in both reactors (Table S2). The increase in acetate concentration had also a significant effect on coulombic efficiency (*CE*) as it decreased from 91% to 57% and from 88% to 46% in bedBES1 and bedBES2, respectively, indicating the emergence of further microbial processes besides current production by *Geobacter* spp. (see Microbial community analysis). Nevertheless, calculations on *CE* are biased by cathodically produced hydrogen that represents an additional substrate for EAM and could promote acetogenesis.^[43]

As expected (see below), cyclic voltammetry (CV) analysis of bedBES showed an undefined shape of *I*-*V* plots before and after inoculation (Figure S3a). This underlined that the internal resistance, and thus poor polarization behavior of bed electrodes impeded analysis by potentiodynamic methods.^[9] By lifting up the CC from the fixed bed during batch operation, CV was performed at the monolithic CC serving as an electrode (Figure S3b). Thereby, one major redox system was observed at a formal potential (E_f) of -340 mV being typically for *Geobacter* spp. based biofilm anodes (Figure S3c).^[26] Although the electrochemical parameters *CE* and E_f exhibited reasonable values, it becomes apparent that the performance of bedBES was low in comparison to prior reported studies. Aelterman *et al.* conducted a similar experiment (e.g., flow system, rod-shaped CC inserted in the bed anode, acetate as sole carbon and energy source) with a smaller reactor setup (0.11 L bed anode volume) but achieved an approximately 30 times higher volumetric current density indicating a better utilization of the bed anode volume for current production (Figure S4).^[35] As the reactor setup of Aelterman *et al.* is considerably smaller, the poor polarization behavior of the granular bed anode presumably didn't come into effect. This resulted in better exploitation of

the bed anode volume and thus a high volumetric current density. Similarly, if an apparent anode area would be calculated considering all granules as ideal spheres, the resulting current density would be 80–160 times smaller than the current density usually obtained by cultivating *Geobacter*-based biofilms at monolithic electrodes (please see calculations and assumptions in Figure S4). These comparisons indicate that the provided bed anode volume is not fully exploited for current production presumably due to limited potential distribution.

Dissecting bed electrodes: CV analysis at different spatial locations

Granules from nine sampling pockets of the longitudinal and transversal axis of each reactor were sampled and analyzed with the e-Clamp during batch operation (granules sampled 33 days after inoculation) and continuous operation (granules sampled 62 days after inoculation). In total, CV analysis of 63 independent granules from different spatial locations with different distances to the CC and medium inflow were performed (see below, Figure 6a,b). The CV analyses of the e-Clamps without granules (e-Clamp control) and with non-inoculated granules (abiotic control) revealed negligible electrochemical signals (Figure S5).

Table 1 summarizes the maximum current density normalized to the respective granule dry weight (j_{max}) obtained from single granules at a polarization of +200 mV during CV. In presence of the substrate acetate, i.e., during turnover conditions, granules from the middle pocket of the top sampling unit (i.e., granules closest to CC; see Figure 6a) produced higher currents during continuous operation ($2.94 \pm 2.08 \mu\text{A mg}^{-1}$) than during batch operation ($1.66 \pm 1.54 \mu\text{A mg}^{-1}$). High currents were also recorded using granules from inner ($2.35 \pm 4.06 \mu\text{A mg}^{-1}$) and outer pockets ($2.40 \pm 1.11 \mu\text{A mg}^{-1}$) of the top sampling unit during continuous but not during batch operation. In contrast, negligible currents were measured for granules from the middle pockets of middle and bottom sampling units during both modes of operation. The remaining

Table 1. Means and standard deviations of formal potentials (E_f) and maximum current densities normalized to dry weight of granules (j_{max}) obtained at +200 mV during turnover CV analysis of both bedBES. Granules were sampled from different pockets of sampling units distributed over the bed anode (see Figure 6a,b). nd = not detected; na = not analyzed.

	Inner pocket				Middle pocket				Outer pocket			
	E_f [mV]	j_{max} [$\mu\text{A mg}^{-1}$]	E_f [mV]	j_{max} [$\mu\text{A mg}^{-1}$]	E_f [mV]	j_{max} [$\mu\text{A mg}^{-1}$]	E_f [mV]	j_{max} [$\mu\text{A mg}^{-1}$]	E_f [mV]	j_{max} [$\mu\text{A mg}^{-1}$]	E_f [mV]	j_{max} [$\mu\text{A mg}^{-1}$]
Top sampling unit	nd (n=3)	0.06 ± 0.03 (n=3)	-378.6 ± 10.9 (n=6)	2.35 ± 4.06 (n=6)	-374.9 ± 8.5 (n=9)	1.66 ± 1.54 (n=9)	-374.3 ± 10.7 (n=12)	2.94 ± 2.08 (n=12)	nd (n=3)	0.04 ± 0.03 (n=3)	-372.0 ± 7.6 (n=6)	2.40 ± 1.11 (n=6)
Middle sampling unit	na	na	na	na	nd (n=6)	0.03 ± 0.01 (n=6)	nd (n=6)	0.04 ± 0.02 (n=6)	na	na	na	na
Bottom sampling unit	na	na	na	na	nd (n=6)	0.03 ± 0.02 (n=6)	nd (n=6)	0.04 ± 0.02 (n=6)	na	na	na	na

pockets, i.e. inner and outer pockets of the middle and bottom sampling units, were not sampled, as the distance to the CC was bigger than for middle pockets of the same sampling units yielding only electrochemically inactive granules. Therefore, it was concluded that granules from these sampling pockets would not exhibit current production as well.

As j_{\max} obtained during turnover conditions can serve as a measure of microbial electrochemical activity (i.e., producing electrical current from acetate oxidation), these CV results demonstrated that the overall charge generation during chronoamperometric operation (Figure 1 for bedBES1 and Figure S1 for bedBES2) of the entire working volume of the bed anode (1.45 L) was actually realized by a minor share of these granules, i.e., by the granules close to the CC. The volume around the sampling pockets of middle and bottom sampling units did not show microbial electrochemical activity while the granules in the inner and outer pockets of the top sampling unit were only active during continuous operation (Table 1).

Longitudinal axis across the bedBES

To shed further light on this limited volume of microbial electrochemical activity within the entire bed anode, further analyses were performed. Graphite granules were sampled during batch and continuous operation from the middle pockets of each sampling unit through the longitudinal axis, i.e., top, middle, and bottom followed by a CV analysis using the e-Clamp. Granules from the middle pocket of the top sampling unit (granules being closest to the CC) of bedBES1 (Figure 2) and bedBES2 (Figure S6) exhibited comparable voltammograms with similar shapes, inflection points, and hence formal potentials of EET (Figure S7) indicating that *Geobacter* spp. were the dominant EAM.^[26] The formal potentials were independent of the mode of operation with $E_f = -374.9 \pm 8.5$ mV for batch and $E_f = -374.3 \pm 10.7$ mV for continuous operation (Table 1). No electrochemical signals, and thus no E_f could be determined for granules from middle and bottom sampling units of both bedBES demonstrating that active EAM were only present in the upper part of bedBES (Figure 2 and Figure S6). Notably, when sampled granules were polarized at +200 mV for 10 h (i.e., BES with the loaded e-Clamp as anode), granules from all pockets of all sampling units of bedBES showed increasing current production indicating microbial growth during this 10 h of chronoamperometry. However, the maximum current production of granules from middle (2.7 ± 1.5 μ A, $n=3$) and bottom (2.3 ± 2.5 μ A, $n=3$) sampling unit were considerably lower than of granules from the top sampling unit (0.36 ± 0.08 mA, $n=3$) after 10 h of cultivation (Figure S8). This further demonstrated that the major share of EAM actively performing EET was present at granules in direct proximity to the CC (roughly corresponds to bed anode volume until 3 cm depth from its surface in this study). In the more distant parts from the CC, the occurrence of EAM and their activity were limited. This can be putatively assigned to limited potential distribution within bed anode and thus electron acceptor limitation representing dead volume within bedBES in

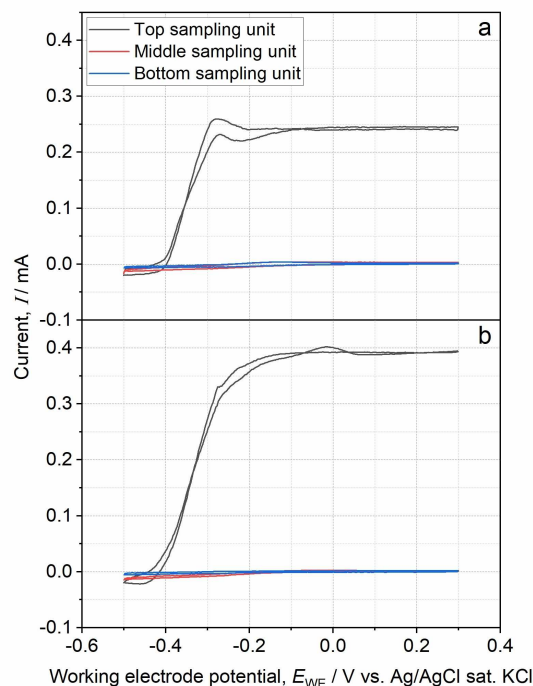


Figure 2. Exemplary cyclic voltammograms (CV) of granules sampled from bedBES1 longitudinal axis under a) batch and b) continuous operation. The CV analyses were performed with the e-Clamp and granules from the middle pocket of the top (black lines), middle (red lines), and bottom sampling unit (blue lines).

terms of microbial electrochemical activity. Interestingly, turnover CV obtained from granules often differed slightly from the sigmoidal shape normally obtained from metabolizing *Geobacter* spp. biofilms cultivated at monolithic electrodes (Figure 2a).^[26]

The presence of a peak pair during turnover CV was already previously observed at granules, but the reasons still need to be deciphered.^[27] The previously discussed oxygen exposure during granule transfer to the BES hosting the e-clamp^[27] could be excluded as the peak pair also occurred under strictly anaerobic conditions (using an anaerobic chamber). We speculate that mainly three processes contributed to the occurrence of the peak pair during CV of sampled granules: i) The small diameter of the granules in conjunction with the pores resulted in a non-planar mass transfer, and thus radial diffusion dominated the CV signal leading to a voltammogram shape that is also found for microparticles.^[48] As acetate transport was increased due to non-planar mass transfer, EAM activity was no longer limited by substrate supply but presumably by metabolizing the substrate and by the transport of electrons to redox moieties (e.g., cytochromes, menaquinones).^[49,50] ii) Planar diffusion and the increased interphase between biofilm and liquid (by removing granules from bed anode with e-Clamp) probably also increased transport of counter ions within biofilm towards its surface decreasing limitations thereby.^[47] iii) By sampling granules, the biofilm was disrupted and part of the biofilm lost its direct

electrochemical contact to the granule (i.e., terminal electron acceptor). Therefore, biofilm parts with no interphases with granules could be regarded as catalytically inactive^[51] in terms of EET, but its redox moieties could still be charged by electrons from acetate oxidation.

In summary, the physical changes due to granule sampling resulted in a shift of kinetic limitations. Instead of acetate and counter ion transport, acetate metabolism and the final EET step (i.e., “gating” electron transfer) putatively became rate-limiting resulting in a charging of redox moieties and the appearance of mixed turnover/non-turnover CV. This hypothesis was further supported by the finding that the “classical” sigmoidal shape of turnover CV always reappeared after 10 h of cultivation at +200 mV (Figure S9A) allowing recovery of electrochemical interphase between biofilm and granules as well as biofilm structure exhibiting its putative typical kinetic limitations (i.e., transport of ions within the biofilm).^[47] In addition to this change of shape, the E_f shifted to more positive potentials (-346.8 ± 13.7 mV) compared to the initial CV (-374.3 ± 10.7 mV; Figure S9B) probably reflecting the more homogeneous potential distribution in single granules compared to bed anode. Consequently, a higher share of cytochromes is in the oxidized state.

Open circuit measurements

During an exemplary batch cycle, the redox potential within bedBES1 was measured across its longitudinal axis by performing open circuit potential (OCP) measurements with three redox sensors close to the top, middle, and bottom sampling unit (see below, Figure 6a). The redox potential of all three sensors decreased with current production. At the end of the batch cycle, as the current decreased to zero, redox potentials of all sensors leveled off to +160 mV being close to the applied potential of +200 mV (Figure 3). During the batch cycle, the

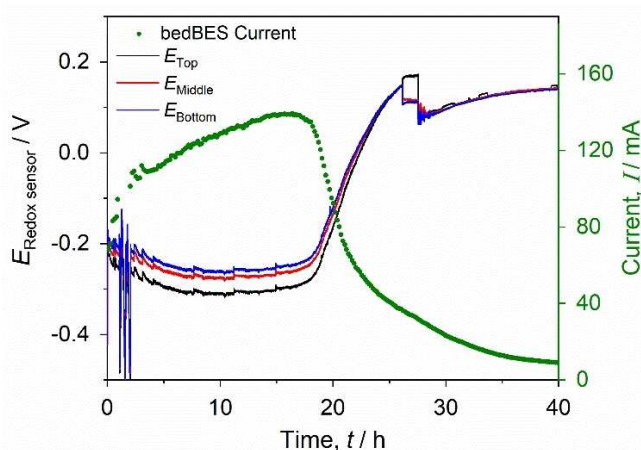


Figure 3. Redox potential recorded during one batch cycle at the top (black), middle (red), and bottom (blue) redox sensor distributed over the longitudinal axis of bedBES1. The green dotted line represents the current production of bedBES1 polarized at +200 mV.

redox potential (registered at $i_{\max} = 96.6 \text{ mA L}^{-1}$) of top sensor (-299 mV) was more negative compared to middle (-263 mV) and bottom sensor (-251 mV). This further indicated a stratification of available redox potential and thus of microbial electrochemical activity within the bed anode. The higher microbial electrochemical activity and thus the promoted growth of EAM close to the top sampling unit (Figure 2) implied higher absolute acetate oxidation rates and higher storage capacities of electrons in intracellular redox moieties resulting in a lower redox potential during OCP measurements.^[52,53] Additionally, the comparable high current production led to a considerable ohmic drop of the available redox potential in the granular bed. Contrarily, the lower concentration of reduced redox moieties led to more positive potentials in parts more distant to the CC. Therefore, the recorded OCP also illustrated the difference in available redox potential due to a poor polarization behavior of bed anode resulting in different activities of EAM within bedBES.

Transversal axis across bedBES

CV analyses were also performed with granules extracted from the inner, middle, and outer pocket of the top sampling units of bedBES1 and bedBES2 following the already described procedure. In accordance with the findings above, current production was high for granules extracted from the middle pocket, but negligible electrochemical signals were detected from granules of the inner and outer pocket during batch operation (Figure 4a and Table 1). Therefore, no E_f could be determined for granules from inner and outer pockets. However, after 10 h of chronoamperometric cultivation at +200 mV, granules from all pockets exhibited an increasing current production. Thereby, the maximum current of granules from the middle pocket were considerably higher (0.12 ± 0.05 mA, $n=3$) compared to granules from inner pocket (0.02 ± 0.01 mA, $n=3$) and outer pocket (0.02 ± 0.02 mA, $n=3$; Figure S10). Apparently, the microbial electrochemical activity was built up more rapidly in the inner and outer pocket of the top sampling unit (Figure S10) compared to middle pockets of middle and bottom sampling units (Figure S8) indicating a higher presence of EAM at the corresponding volumes. Presumably, the redox potential was more positive close to the top sampling unit of bedBES compared to pockets of middle and bottom sampling units as the respective pockets were closer to the CC. During continuous operation, granules from all pockets of the top sampling unit showed current production (Figure 4b) and similar E_f could be determined (-378.6 ± 10.9 mV, -374.3 ± 10.7 mV, and -372.0 ± 7.6 mV for inner, middle, and outer pockets, respectively; Table 1) being comparable to previously determined E_f (section longitudinal axis across the bedBES). These results support the assumption of a limited potential distribution and thus poor polarization behavior within bed anode of bedBES as all pockets from the top sampling unit were closer to the CC compared to the pockets from middle and bottom sampling unit. Thus, these pockets experienced a more positive potential being required for higher microbial electrochemical activity.

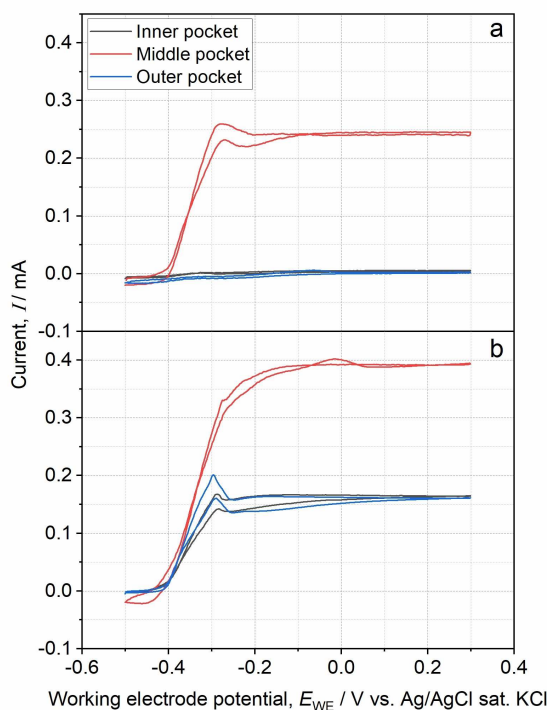


Figure 4. Exemplary cyclic voltammograms (CV) of graphite granules extracted from bedBES1 transversal axis during a) batch and b) continuous operation. The CV analysis was performed directly after sampling granules with the e-Clamp from the inner (black), middle (red), and outer (blue) pockets of the top sampling unit. The scan rate was 1 mVs^{-1} (3^{rd} scans are shown).

Nevertheless, granules from inner and outer pockets of the top sampling unit needed more time for exhibiting microbial electrochemical activity than granules from the middle pocket that already produced considerable current during batch operation (Figure 4a). As the inner and outer pockets were more distant to the CC than the middle pocket, the available redox potential was lower, and thus the driving force for EET was lower resulting in slower growth of EAM. It is also of note that the CV of all sampled granules from the top sampling unit exhibited the additional peak pair and reshaped to the “classical” sigmoidal curve after 10 h of chronoamperometric cultivation (Figure S9; see discussion above).

Microbial community analysis

The microbial community composition was determined using was determined by performing terminal restriction fragment length polymorphism (TRFLP) analysis in order to decipher structure-function relationships. During batch operation, one single terminal restriction fragment (TRF, 213 bp) dominated the bacterial community of all granules obtained from all sampling pockets of both reactors with an abundance of $93.0 \pm 3.9\%$ (Figure 5a for bedBES1 and S11A for bedBES2). This TRF could be assigned to *Geobacter* spp.^[43] representing the

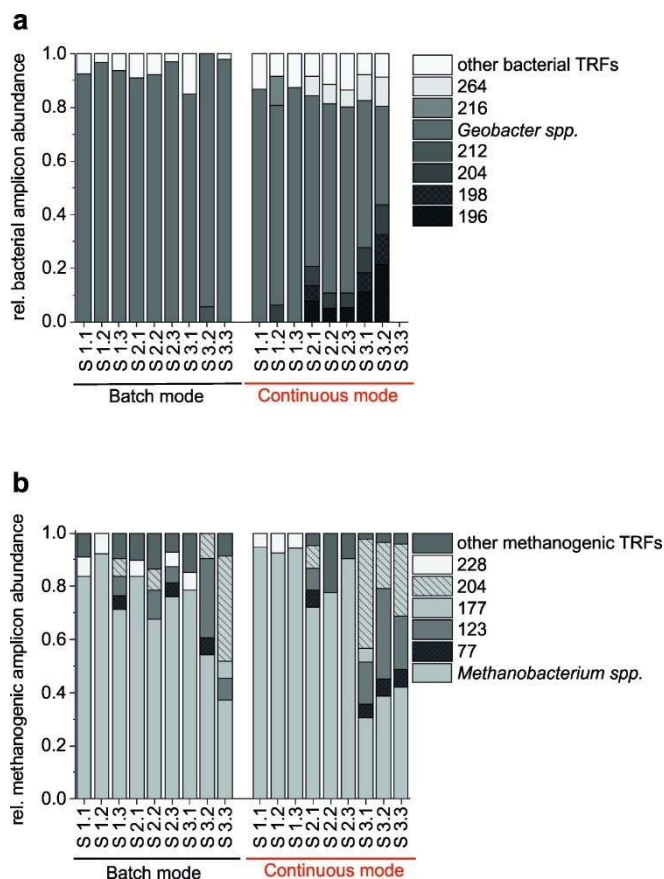


Figure 5. Microbial community composition within bedBES1 determined with TRFLP for a) the bacterial (restriction enzyme *HaeIII*) and b) the methanogenic community (restriction enzyme *MwoI*). Granules from all pockets of the top (S 1.1, S 1.2, and S 1.3 for inner, middle, and outer sampling pocket, respectively), middle (S 2.1, S 2.2, and S 2.3), and bottom (S 3.1, S 3.2, and S 3.3) sampling unit were analyzed. Sampling was conducted at day 33 and day 62 for obtaining results for batch and continuous operation, respectively. No bacterial DNA could be extracted from sampling pocket S 3.3 during batch cultivation.

typically enriched EAM at monolithic electrodes using identical cultivation conditions (i.e., acetate as sole carbon and energy source, polarized solid electron acceptor).^[30,31,54,55] The identification of *Geobacter* spp. in all sampling pockets via TRFLP, although no electrochemical signals could be detected in few sampling pockets (Table 1), can be explained with sensitivity differences between the used methods (i.e., electrochemistry and TRFLP analysis) and the capacitive properties of graphite granules.^[17] Although large portions of the bed anode were not sufficiently polarized, *Geobacter* spp. were apparently able to oxidize acetate and store metabolically received electrons in the electric double layer of the granule pores in these zones.^[17] However, as the capacitance of granules is limited, the metabolic activity and growth of *Geobacter* spp. were limited as well. Thus, the formed biomass was not sufficient to cause a detectable electrochemical signal with the used electrochemical setup although DNA from the model EAM was extracted.

The continuous operation provoked a general decrease in abundance of *Geobacter* spp. in all sampling pockets of both

bedBES ($67.1 \pm 14.8\%$). However, the abundance of *Geobacter* spp. in all pockets of the top sampling unit (i.e., at granules close to CC) were considerably higher ($83.0 \pm 6.6\%$) compared to pockets of middle and bottom sampling unit ($58.4 \pm 9.7\%$) of both bedBES. Due to the poor polarization of granules more distant from the CC, the availability of a terminal electron acceptor (i.e., anode) is decreased in these zones. Thus, the selection advantage for efficient EAM (e.g., *Geobacter* spp.) is reduced leading to the emergence of further bacterial species. Furthermore, the higher substrate load during continuous operation, especially with 20 mM acetate, likely contributed to this observation. *Geobacter* spp. is assumed to outcompete other anaerobic acetate-consuming microorganisms due to a kinetic advantage in acetate uptake, especially when using solid terminal electron acceptors (Table S12). However, for monolithic electrodes, it is also known that the acetate uptake of *Geobacter* spp. saturates around 5–10 mM acetate.^[43,56] Therefore, “acetate leftovers” are available for other microorganisms in case of high acetate loads resulting in a more diverse microbial community. TRFLP analysis is indeed a reliable and fast screening method for analyzing microbial composition,^[57] but for an accurate quantification of microorganisms that also allows comparison of different microbial domains, other techniques, such as qPCR, are better suited.^[44]

Similarly, TRFLP analysis of the methanogenic community revealed that almost all sampling pockets of bedBES1 (Figure 5b) and bedBES2 (Figure S11B) were dominated by one archaeal genus, *Methanobacterium*, during batch ($71.7 \pm 15.9\%$) and continuous ($70.3 \pm 24.7\%$) operation.^[58] Hydrogenotrophic methanogens are commonly found in one-chamber reactors as their substrates, hydrogen and carbon dioxide, are provided by the cathode and acetate oxidation performed by *Geobacter* spp., respectively.^[44,59,60] Interestingly, the abundance of *Methanobacterium* seemingly decreased downwards through the longitudinal axis of both reactors during batch operation ($82.5 \pm 8.6\%$, $75.9 \pm 6.6\%$, and $56.8 \pm 16.9\%$ for top, middle, and bottom sampling unit, respectively) parallel to an increase in the diversity of methanogenic archaea. This effect was intensified under continuous operation (Figure 5b for bedBES1 and Figure S11B for bedBES2). The TRFLP analysis also indicated that further methanogenic families occurred in bedBES, e.g., *Methanomicrobiaceae* (TRF 204) and *Methanosarcinaceae* (TRF 123).^[58] However, by performing sequencing, only the presence of *Methanobacterium* spp. and *Methanosarcina* spp. (for bedBES2, Figure S11B) could be revealed. The availability of cathodically produced hydrogen and the reactor geometry constituted a gradient with more hydrogen close to the cathode and less hydrogen at the bottom sampling unit. During continuous operation, the gradient increased as the flow direction is opposite to the hydrogen supply. Therefore, different metabolite gradients were formed in the bed anode during batch and continuous operation selecting for different methanogenic communities.

The apparent lack of acetoclastic methanogens in all reactor setups confirms the energetic and kinetic disadvantage thereof compared to hydrogenotrophic methanogens and *Geobacter* spp.^[61,62]

Conclusions

To analyze the redox potential distribution and the associated spatial distribution of microbial electrochemical activity within bed anodes bedBES were constructed and operated with a model process. In addition, these housing-integrated sampling units allowed minimally invasive sampling of granules ($n=63$). In general, a high number of independent replicates ($n \geq 3$) is not only desired but is also needed to draw quantitative conclusions and derive structure-function relationships to allow engineering and even steering of specific processes towards application. However, experimental requirements (i.e., medium supply during continuous mode, simultaneous electrochemical analysis of all sampled granules) limited the investigation to two representative reactor replicates. Single granules were electrochemically analyzed with the e-Clamp and by molecular biological analyses for obtaining information on thermodynamics of EET and the microbial composition, respectively. By performing cyclic voltammetry with single granules sampled from different locations within the bed anode, it was demonstrated that the microbial electrochemical activity was stratified and only situated in close vicinity to the current collector during batch and continuous operation. Consequently, the provided bed anode volume was only partially used by EAM for current production, resulting in comparable low volumetric current densities. Microbial community analysis supports this finding by showing higher relative abundances of *Geobacter* spp. close to the current collector. Although the experiment were conducted with an exemplary model system for EAM (i.e., bedBES were inoculated with *Geobacter* spp. enrichment biofilm and acetate as sole carbon source), it can be assumed that the observed effects are more pronounced in reactors with more complex substrates (e.g., wastewater or treating pollutants) as the diverse selection pressures may hamper the growth of EAM.^[28] Furthermore, the limited potential distribution presumably leads to a selection of more efficient EAM (e.g., *Geobacter* spp.), resulting in a less diverse and thus less stable and flexible (electroactive) microbiome.^[63,64] For analyzing the development of the microbial community within fixed bedBES, the experimental system needs further refinements for allowing a finer resolution in time and space, as well as accounting for the influence of the therefore more often required sampling events.^[64]

CV results suggested that the reported space-time yields and volumetric rates of bedBES that were designed with simple current collectors (e.g., rod) only sparsely electrically contacting the granular bed were actually achieved by a small volume within the bedBES, owing to a poor potential distribution. This limitation in “active” volume may be avoided with proper bed electrode engineering and designed execution in pursuit of a better potential distribution, that is, by incorporating a wide-ranging current collector that covers the longitudinal and transversal axes of bed electrodes. Consequently, an optimized polarization scenario would support the electron exchange between EAM and the bed electrode, decreasing the limitation thereby and facilitating metabolic processes. For instance, comparable cheap corrosion-resistant metal meshes with mesh

sizes of only few centimeters that are arranged and electrically connected in a 3D structure (e.g., like a cage) could act as granular bed backbone. As a result, the occurrence of dead volumes within the bed electrodes would be drastically reduced and thus the treatment performance of, e.g., with organics and/or pollutants contaminated waste, ground, and surface water improved.^[65] This approach would be especially suitable for low-cost scenarios (e.g., sediment BES), however, in scenarios with limited mass transfer, fluidized bed reactors may represent the better option.^[9] The presented study not only establishes a relation between electrochemical parameters, microbial selection in ecological niches, and the performance of EAM within bed electrodes but also illustrates the enhancement opportunities of 3D-granular electrodes.

Experimental Section

General conditions

All chemicals were of analytical grade and were supplied by Carl Roth GmbH (Karlsruhe, Germany) and Merck KGaA (Darmstadt, Germany). Deionized water (Merck Chemicals GmbH, Darmstadt, Germany) was used in the preparation of all solutions. If not stated otherwise, all potentials provided in this article refer to Ag/AgCl sat. KCl (+197 mV vs. standard hydrogen electrode, SHE). All provided volumetric current densities refer to the volume of the bed anode.

Setup of bedBES

The bedBES (Figure 6a) were based on unplasticized polyvinyl chloride (PVC-U) tube (total length 34 cm, inner diameter 10.2 cm, Marley Deutschland GmbH, Wunstorf, Germany) defining a single tubular chamber of a total volume of 2.70 L. Bottom and lid of the bedBES were tailor-made of PVC-U. The counter electrode consisted of a titanium mesh with a geometric surface area of 300 cm² (Goodfellow GmbH, Friedberg, Germany). The bed anode acted as a working electrode (WE) and was constituted of 1500 g of unstirred graphite granules (enViro-cell Umwelttechnik GmbH, Oberursel, Germany; diameters from 1 to 5 mm, obtained by mechanical sieving). The bed anode occupied from the bottom of the reactor 20 cm height (i.e., 1.45 L). A graphite rod (1 cm diameter, CP-Graphitprodukte GmbH, Wachtberg, Germany) was connected to 0.5 mm diameter titanium wire (Goodfellow GmbH, Friedberg, Germany) and the connection was sealed with epoxy resin (HT2, R&G Faserverbundwerkstoffe, Germany). The rod was vertically embedded 1.5 cm deep into the bed acting as a current collector (CC). Above the granular bed, the rod was insulated with epoxy resin (HT2, R&G Faserverbundwerkstoffe, Germany). This approach followed the usual strategy for electrochemically connecting bedBES.^[14,20] The reference electrode (Ag/AgCl sat. KCl, SE11, Xylem Analytics Germany Sales GmbH & Co. KG Sensortechnik Meinsberg, Meinsberg, Germany) was placed parallel to the current collector at a distance of 0.5 cm. It was placed 0.5 cm above the granular bed in the liquid phase (Figure 6a).

The bedBES contained three sampling units made of PVC-U at different heights perpendicularly to the longitudinal axis (Figure 6b). Each sampling unit consisted of three cylindrical parts. The outermost part was fixed to the reactor with Tangit PVC-U (Henkel AG & Co. KGaA, Düsseldorf, Germany) and the inner parts were rotatable and removable. At the front end and back end of the innermost cylinder, O-ring seals were added for assuring anoxic

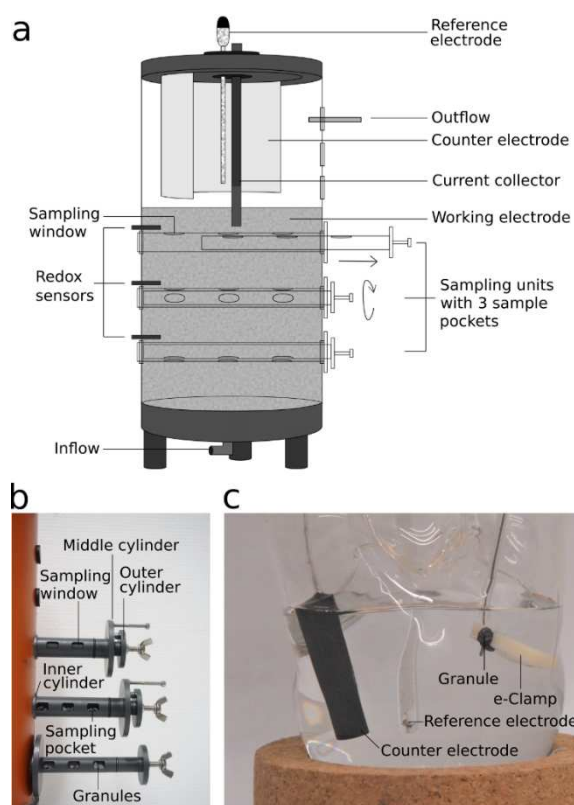


Figure 6. a) Scheme of a fixed-bed electrode bioelectrochemical system (bedBES). b) Picture showing a section of the constructed bedBES with the three minimally invasive sampling units (top, middle, bottom) at different heights of the longitudinal axis of the bedBES. Each sampling unit provided access to granules in three different points of the transversal axis of bedBES by rotating the middle cylinder of the sampling units in order to have an open configuration of the sampling units. Thereby, the granules fell through the sampling windows of the outer and middle cylinder into the sampling pockets. Subsequently, the inner cylinder of the sampling unit was pulled allowing a minimally invasive sampling of granules by using the e-Clamp. c) e-Clamp inserted into a bioelectrochemical reactor allowing cyclic voltammetry of single granules.

conditions within bedBES during sampling. Each sampling unit provided access to granules in three different points of the transversal axis by means of sampling windows (12 mm length, 8 mm width) allowing harvesting several granules. During operation, all parts of the sampling units were completely inserted in the bedBES with closed sampling windows. The three-part cylindrical system of sampling units provided access to the granules (without exposing the bed anode to the external atmosphere) by manual rotation of the inner cylinders. Once the granules fell through the windows into the pockets (12 mm length, 8 mm width, 4 mm depth) of the inner cylinder, they could be sampled from the reactor while maintaining anoxic conditions. Redox sensors (i.e., graphite rods, 0.5 cm diameter, CP-Graphitprodukte GmbH, Wachtberg, Germany) were also inserted beside each of the sampling units (until 3 cm depth). A second reference electrode placed close to the first reference electrode allowed to monitor the redox potential of these three redox sensors independently of the polarized electrochemical circuit. The bed anode occupied a total volume of 1.6 L including the three sampling units. Each of the sampling units had a volume of 0.05 L.

BedBES inoculation and operation

All experiments were carried out under potentiostatic control using a multi-channel potentiostat/galvanostat (MPG-2, Bio-Logic Science Instruments, Claix, France) and the medium was artificial wastewater,^[66] supplemented with sodium acetate (10 or 20 mM, as specified) acting as sole carbon source. Vitamin and trace metal solutions were added according to a previously reported method.^[67] Prior to the start of the experiment, 1.5 L medium was purged with nitrogen for 30 min and anaerobically transferred to bedBES. After 85 h of abiotic operation, the two bedBES were inoculated with secondary *Geobacter* spp. enrichment biofilm cultivated in a two-chamber reactor (*Geobacter* abundance $\approx 90\%$) as described elsewhere.^[43,44,68]

Thereby, the biofilm was sampled with a sterile spatula and transferred into a falcon tube containing 10 mL medium. Subsequently, the biofilm was homogenized by vortexing for 30 s. The resulted suspension was diluted in 1.5 L medium previously purged with nitrogen for 30 min to remove oxygen (final OD of 0.03). Afterward, the total media was anaerobically pumped through the inflow port located at the bedBES bottom. The temperature was maintained at 35 °C (Incubator Hood TH 15, Edmund Bühler GmbH, Bodelshausen, Germany). The medium was replaced periodically when current production dropped to zero. After 45 days in batch operation, the bedBES were operated in continuous mode for 15 days resulting in a total experimental duration of 2 months. During continuous mode, the acetate concentration was increased from 10 to 20 mM after 7 days of continuous operation. The medium was pumped with a peristaltic pump (Watson-Marlow GmbH, Rommerskirchen, Germany) through the inflow port at the bedBES bottom with a hydraulic retention time (HRT) of 1.0 ± 0.1 d. Outflow was at the top of the reactor at a height of 32 cm.

BedBES were chronoamperometrically operated (CA) at 200 mV. Cyclic voltammograms were performed between +300 V and -500 mV at a scan rate of 1 mVs^{-1} . The third cycle, showing a quasi-steady state performance, was used for data analysis in accordance with.^[69] During batch (33 days after inoculation) and continuous operation (62 days after inoculation), granules from different sampling pockets of the longitudinal and transversal axis of bedBES were sampled via the sampling units and analyzed with the e-Clamp. Samples from influent and effluent streams were taken regularly.

Electrochemical analysis of single granules

For studying single granules sampled from bedBES, the e-Clamp was used in four-neck round-bottom flasks as described previously.^[68] The e-Clamp was a tailor-made clamp printed from acrylonitrile butadiene styrene (ABS; Innofil3D B.V., Emmen, The Netherlands) with a 3D printer (Ultimaker 2+, Ultimaker B.V., Utrecht, The Netherlands) acting as the contacting support for a platinum plate (1 mm^2) representing the CC. The tailor-made clamp and the CC form the e-Clamp that, together with single granules, constituted a working electrode (Figure 6c). The resistance between the CC and granule was always below 5Ω . Counter electrodes were made of graphite rods (CP-Graphitprodukte GmbH, Wachtberg, Germany) with a total projected surface area of 4.7 cm^2 . The reference electrode was identical as used for the bedBES. To avoid diffusion limitations, the cell was stirred at 140 rpm using a magnetic stirrer. In total, CV of 63 single granules were recorded (three cycles were performed between +300 and -500 mV at a scan rate of 1 mVs^{-1} , the third cycle was used for data analysis). Some granules were chronoamperometrically polarized at +200 mV for 10 h after CV for further analyzing the activity of single granules. Control measurements were performed using an

identical setup but without graphite granules (i.e., e-Clamp control) and with abiotic, not inoculated, granules (i.e., abiotic control). Identically to the bedBES, all analyses were performed using 250 mL artificial wastewater according to a previously reported method,^[66] with 10 mM sodium acetate, vitamin, and trace metal solutions.^[67] Before the start of the experiment, the solution was purged with nitrogen for 30 min to ensure anaerobic conditions. The temperature was maintained at 35 °C (Incubator Hood TH 15, Edmund Bühler GmbH, Germany).

Analytical methods and calculations

Acetate consumption was monitored using high-performance liquid chromatography (HPLC, Shimadzu Scientific Instruments, Kyoto, Japan) equipped with refractive index detector RID-10 A and a Hi-Plex H column ($300 \text{ mm} \times 7.7 \text{ mm}$ ID, $8 \mu\text{m}$ pore size, Agilent Technologies, Santa Clara, USA), and a pre-column (Carbo-H 4 $\text{mm} \times 3 \text{ mm}$ ID, Security Guard, Torrance, Phenomenex). Isocratic elution at 50 °C with 5 mM H_2SO_4 was set at 0.5 mL min^{-1} for 30 min. Peak identification and calibration of acetate was carried out with external standards (0.1 mM to 22.2 mM, six-point calibration; calibration limit was 0.1 mM, $R^2 = 0.99$). Samples were centrifuged at $13,000 \times g$ for 5 min and filtered with a $0.2 \mu\text{m}$ nylon filter. HPLC analyses were performed immediately after sampling and acetate was the only analyte that could be detected in the liquid phase. Acetate consumption data was used to determine coulombic efficiency (CE). The CE is the ratio of produced charge, Q , and the theoretical charge production from acetate oxidation, Q_{theory} , assuming that all consumed acetate is converted into current [Eq. (1)]. Thus, CE describes the overall electron efficiency of EAM.

$$CE = \frac{Q}{Q_{\text{theory}}} \times 100\% \quad (1)$$

where Q is produced charge derived from the integration of current i over time t [Eq. (2)]:

$$Q(t) = \int_0^t i dt \quad (2)$$

and Q_{theory} is the theoretical charge derived from acetate consumption determined by HPLC analysis [Eq. (3)]:

$$Q_{\text{theory}} = \Delta c \times V \times z \times F \quad (3)$$

Δc is change in acetate concentration, V is volume, z is the number of transferred electrons (8 in case of acetate), and F is the Faraday constant ($96,485.3 \text{ C mol}^{-1}$). The dry weight of single granules were determined after CV measurements with e-Clamp by drying the granules at 80 °C for 12 h. Granules were stored in a desiccator until weight stabilization before weight determination.

Microbial characterization

The microbial community was analyzed on DNA level for bacteria and methanogenic archaea with TRFLP. DNA of 3–4 granules per sample was extracted with the NucleoSpin Tissue Kit (Macherey-Nagel, Dürren, Germany) following the manufacturer instructions. Genomic DNA was finally eluted in $50 \mu\text{L}$ elution buffer and the concentration was measured with Nano Drop™ One (Thermo Fisher Scientific, Waltham, USA). The bacterial community was analyzed by using the primers UniBac27f (FAM-labeled) and Univ1492r for amplifying a partial sequence of the 16S rRNA of

bacteria.^[70] Primers *mias* and *mcrA_rev* (FAM-labeled) were used for amplifying the archaeal *mcrA* gene (subunit A of methyl coenzyme M reductase).^[71] The PCR Master Mix contained 6.25 μL enzyme mix (MyTaq HS Red Mix, 2x, Bioline GmbH, Luckenwalde, Germany), 0.25 μL of each primer (5 pmol μL^{-1} , MWG Biotech AG, Ebersberg, Germany), 4.75 μL nuclease-free water, and 1 μL genomic DNA (in general, ca. 3 to 15 ng, in exceptional cases 50–600 ng). The PCR cycle parameters were as follows: bacteria: 1 min at 95 °C, 25 cycles of 15 s at 95 °C, 15 s at 54 °C, and 2 min at 72 °C, followed by a 10 min extension step at 72 °C;^[72] archaea: 1 min at 95 °C, 5 initial cycles of 15 s at 95 °C, 15 s at 48 °C and 30 s at 72 °C, including a ramp rate of 0.1 °C s⁻¹ from the annealing to the extension temperature, 20 cycles of 15 s at 95 °C, 15 s at 52 °C, and 30 s at 72 °C followed by a 10 min extension step at 72 °C.^[73] PCR products were purified (Sure Clean Plus, Bioline GmbH) and digested with restriction endonucleases *HaeIII* and *RsaI* for 16S rRNA genes of bacteria and *MwoI* and *MseI* for *mcrA* of methanogenic archaea (New England Biolabs GmbH, Frankfurt am Main, Germany). Product precipitation (EDTA/EtOH) and TRFLP analysis was performed using an ABI PRISM Genetic Analyzer 3130xI (Applied Biosystems, Foster City, USA). Size standards for 16S rRNA and *mcrA* were MapMarker 1000 (BioVentures Inc., Murfreesboro, USA) and Red DNA Size Standard (MC LAB, South San Francisco, USA), respectively. For the methanogenic community, a standard sequencing procedure was performed to assign the major TRFs to operational taxonomic units.^[72] In brief, unlabeled PCR products were cloned with Qiagen PCR Cloning Kit (Qiagen, Hilden, Germany) following the manufacturer's instruction. Clones were selected for further PCR amplification using M13 primers (cycle parameters: 1 min at 95 °C and 25 cycles of 15 s at 95 °C, 15 s at 55 °C and 2 min at 72 °C followed by a 10 min extension step at 72 °C). Subsequently, the TRF length of 160 clones were analyzed. 64 clones without known TRF assignments were then sequenced using an ABI PRISM Genetic Analyzer 3130xI (Applied Biosystems, Germany).

Data analysis and statistics

Mean and standard deviation of maximum current density (j_{max} ; measured at +200 mV during the forward and backward scan of single granule CV), dry weight and formal potentials (E_f) were calculated with $n \geq 3$.

Acknowledgements

This work was supported by the Helmholtz-Association within the Research Program Renewable Energies. Open access funding enabled and organized by Projekt DEAL.

Conflict of Interest

The authors declare no conflict of interest.

Keywords: 3D printing · cyclic voltammetry · electrochemistry · electrode materials · electron transfer

[1] U. Schröder, F. Harnisch, L. T. Angenent, *Energy Environ. Sci.* **2015**, *8*, 513–519.

[2] D. R. Lovley, *Energy Environ. Sci.* **2011**, *4*, 4896–4906.

- [3] R. M. Snider, S. M. Strycharz-Glaven, S. D. Tsoi, J. S. Erickson, L. M. Tender, *Proc. Natl. Acad. Sci. USA* **2012**, *109*, 15467–15472.
- [4] N. S. Malvankar, M. T. Tuominen, D. R. Lovley, *Energy Environ. Sci.* **2012**, *5*, 5790–5797.
- [5] S. Chen, S. A. Patil, R. K. Brown, U. Schröder, *Appl. Energy* **2019**, 233–234, 15–28.
- [6] F. Aulenta, S. Puig, F. Harnisch, *Microb. Biotechnol.* **2018**, *11*, 18–19.
- [7] S. Kerzenmacher in *Adv. Biochem. Eng. Bioelectrosynthesis* (Eds.: F. Harnisch, D. Holtmann), Springer Nature Switzerland, **2019**, pp. 135–180.
- [8] Y. Y. Yu, D. D. Zhai, R. W. Si, J. Z. Sun, X. Liu, Y. C. Yong, *Int. J. Mol. Sci.* **2017**, *18*, 90.
- [9] J. R. Quejigo, Q. Sara, T. Sanz, A. Esteve-Núñez, F. Harnisch, *ChemTexts* **2019**, *5*, 4.
- [10] S. Tejedor-Sanz, P. Fernández-Labrador, S. Hart, C. I. Torres, A. Esteve-Núñez, *Front. Microbiol.* **2018**, *9*, 378.
- [11] D. D. Liu, M. Roca-Puigros, F. Geppert, L. Caizán-Juanarena, S. P. N. Ayudthaya, C. Buisman, A. ter Heijne, *Front. Bioeng. Biotechnol.* **2018**, *6*, 78.
- [12] Y. Feng, H. Lee, X. Wang, Y. Liu, W. He, *Bioresour. Technol.* **2010**, *101*, 632–638.
- [13] I. Rabaey, W. Ossiur, M. Verhaege, W. Verstraete, *Water Sci. Technol.* **2005**, *52*, 515–523.
- [14] A. Aguirre-Sierra, T. Bacchetti-De Gregoris, A. Berná, J. J. Salas, C. Aragón, A. Esteve-Núñez, *Environ. Sci. Water Res. Technol.* **2016**, *2*, 984–993.
- [15] T. M. Huggins, H. Wang, J. Kearns, P. Jenkins, Z. J. Ren, *Bioresour. Technol.* **2014**, *157*, 114–119.
- [16] T. M. Huggins, J. J. Pietron, H. Wang, Z. J. Ren, J. C. Biffinger, *Bioresour. Technol.* **2015**, *195*, 147–153.
- [17] C. Borsje, D. Liu, T. H. J. A. Sleutels, C. J. N. Buisman, A. ter Heijne, *J. Power Sources* **2016**, *325*, 690–696.
- [18] N. Ibl, *Compr. Treatise Electrochem.* **1983**, 239–315.
- [19] J. S. Newman, C. W. Tobias, *J. Electrochem. Soc.* **1962**, *109*, 1183–1191.
- [20] K. Rabaey, P. Clauwaert, P. Aelterman, W. Verstraete, *Environ. Sci. Technol.* **2005**, *39*, 8077–8082.
- [21] H. T. Tran, J. H. Ryu, Y. H. Jia, S. J. Oh, J. Y. Choi, D. H. Park, D. H. Ahn, *Water Sci. Technol.* **2010**, *61*, 1819–1827.
- [22] X. Zhang, J. Shi, P. Liang, J. Wei, X. Huang, C. Zhang, B. E. Logan, *Bioresour. Technol.* **2013**, *142*, 109–114.
- [23] M. Di Lorenzo, T. P. Curtis, I. M. Head, S. B. Velasquez-Orta, K. Scott, *Water Sci. Technol.* **2009**, *60*, 2879–2887.
- [24] A. Cardenas-Robles, E. Martinez, I. Rendon-Alcantar, C. Frontana, L. Gonzalez-Gutierrez, *Bioresour. Technol.* **2013**, *127*, 37–43.
- [25] J. Liu, F. Zhang, W. He, X. Zhang, Y. Feng, B. E. Logan, *J. Power Sources* **2014**, *261*, 278–284.
- [26] K. Fricke, F. Harnisch, U. Schröder, *Energy Environ. Sci.* **2008**, *1*, 144–147.
- [27] J. R. Quejigo, L. F. M. Rosa, F. Harnisch, *Electrochem. Commun.* **2018**, *90*, 78–82.
- [28] C. Koch, K. J. Huber, B. Bunk, J. Overmann, F. Harnisch, *NPJ Biofilms Microbiomes* **2019**, *5*, 27.
- [29] X. Zhang, K. Rabaey, A. PrévotEAU, *ChemElectroChem* **2019**, *6*, 1921–1925.
- [30] C. I. Torres, R. Krajmalnik-Brown, P. Parameswaran, A. K. Marcus, G. Wanger, Y. A. Gorby, B. E. Rittmann, *Environ. Sci. Technol.* **2009**, *43*, 9519–9524.
- [31] A. S. Commault, G. Lear, M. A. Packer, R. J. Weld, *Bioresour. Technol.* **2013**, *139*, 226–234.
- [32] P. G. Dennis, B. Viridis, I. Vanwonterghem, A. Hassan, P. Hugenholtz, G. W. Tyson, K. Rabaey, *Sci. Rep.* **2016**, *6*, 39114.
- [33] C. Koch, F. Harnisch, *ChemElectroChem* **2016**, *3*, 1282–1295.
- [34] B. Korth, F. Harnisch, *Front. Microbiol.* **2019**, *10*, 1352.
- [35] P. Aelterman, S. Freguia, J. Keller, W. Verstraete, K. Rabaey, *Appl. Microbiol. Biotechnol.* **2008**, *78*, 409–18.
- [36] L. A. Zacharoff, C. H. Chan, D. R. Bond, *Bioelectrochemistry* **2016**, *107*, 7–13.
- [37] L. Peng, S.-J. You, J.-Y. Wang, *Biosens. Bioelectron.* **2010**, *25*, 2530–2533.
- [38] C. E. Levar, C. H. Chan, M. G. Mehta-Kolte, D. R. Bond, *mBio* **2014**, *5*, e02034.
- [39] R. A. Yoho, S. C. Papat, C. I. Torres, *ChemSusChem* **2014**, *7*, 3413–3419.
- [40] A. Hirose, T. Kasai, M. Aoki, T. Umemura, K. Watanabe, A. Kouzuma, *Nat. Commun.* **2018**, *9*, 1083.
- [41] B. Boehrer, M. Schultze, *Rev. Geophys.* **2008**, *46*, RG2005.
- [42] D. R. Lovley, D. E. Holmes, K. P. Nevin, *Adv. Microb. Physiol.* **2004**, *49*, 219–286.

- [43] B. Korth, J. Kretzschmar, M. Bartz, A. Kuchenbuch, F. Harnisch, *PLoS One* **2020**, *15*, e0234077.
- [44] B. Korth, A. Kuchenbuch, F. Harnisch, *ChemElectroChem* **2020**, *7*, 3720–3724.
- [45] C. Moß, A. Behrens, U. Schröder, *ChemSusChem* **2019**, 582–589.
- [46] P. Chong, B. Erable, A. Bergel, *Bioresour. Technol.* **2019**, *289*, 121641.
- [47] S. C. Popat, C. I. Torres, *Bioresour. Technol.* **2016**, *215*, 265–273.
- [48] F. Scholz, U. Schröder, R. Gulaboski, A. Doménech-Carbó, *Electrochemistry of Immobilized Particles and Droplets*, Springer International Publishing, **2015**.
- [49] S. M. Strycharz, A. P. Malanoski, R. M. Snider, H. Yi, D. R. Lovley, L. M. Tender, *Energy Environ. Sci.* **2011**, *4*, 896–913.
- [50] B. Korth, L. F. M. Rosa, F. Harnisch, C. Picioreanu, *Bioelectrochemistry* **2015**, *106*, 194–206.
- [51] L. Peng, X. T. Zhang, J. Yin, S. Y. Xu, Y. Zhang, D. T. Xie, Z. L. Li, *Electrochim. Acta* **2016**, *191*, 743–749.
- [52] A. Esteve-Núñez, J. Sosnik, P. Visconti, D. R. Lovley, *Environ. Microbiol.* **2008**, *10*, 497–505.
- [53] G. D. Schrott, P. S. Bonanni, J. P. Busalmen, *Electrochim. Acta* **2019**, *303*, 176–182.
- [54] X. Zhu, M. D. Yates, M. C. Hatzell, H. A. Rao, P. E. Saikaly, B. E. Logan, *Environ. Sci. Technol.* **2014**, *48*, 1352–1358.
- [55] A. S. Commault, G. Lear, R. J. Weld, *Environ. Sci. Technol.* **2014**, *48*, 14851–14852.
- [56] J. Kretzschmar, L. F. M. Rosa, J. Zosel, M. Mertig, J. Liebetrau, F. Harnisch, *Chem. Eng. Technol.* **2016**, *39*, 637–642.
- [57] J. De Vrieze, U. Z. Ijaz, A. M. Saunders, S. Theuerl, *Sci. Rep.* **2018**, *8*, 16818.
- [58] F. Bühligen, R. Lucas, M. Nikolausz, S. Kleinsteußer, *Anaerobe* **2016**, *39*, 114–116.
- [59] H. S. Lee, C. I. Torres, P. Parameswaran, B. E. Rittmann, *Environ. Sci. Technol.* **2009**, *43*, 7971–7976.
- [60] M. Siegert, X. F. Li, M. D. Yates, B. E. Logan, *Front. Microbiol.* **2015**, *5*, 778.
- [61] N. R. Buan, *Emerg. Top. Life Sci.* **2018**, *2*, 629–646.
- [62] B. Michał, P. Gagat, S. Jabłoński, J. Chilimoniuk, M. Gaworski, P. Mackiewicz, Ł. Marcin, *Environ. Microbiol. Rep.* **2018**, *10*, 378–382.
- [63] D. Y. A. Esquivel, Y. Guo, R. K. Brown, S. Müller, U. Schröder, F. Harnisch, *ChemElectroChem* **2020**, *7*, 989–997.
- [64] C. Koch, B. Korth, F. Harnisch, *Microb. Biotechnol.* **2018**, *11*, 22–38.
- [65] N. Pous, B. Korth, M. Osset-Álvarez, M. D. Balaguer, F. Harnisch, S. Puig, *Bioresour. Technol.* **2021**, *319*, 124221.
- [66] J. R. Kim, B. Min, B. E. Logan, *Appl. Microbiol. Biotechnol.* **2005**, *68*, 23–30.
- [67] W. E. Balch, G. E. Fox, L. J. Magrum, C. R. Woese, R. S. Wolfe, *Microbiol. Rev.* **1979**, *43*, 260–296.
- [68] C. Gimkiewicz, F. Harnisch, *J. Visualization* **2013**, 50800.
- [69] F. Harnisch, S. Freguia, *Chem. Asian J.* **2012**, *7*, 466–75.
- [70] D. J. Lane, in *Nucleic Acid Tech. Bact. Syst.* (Eds.: E. Stackebrandt, M. Goodfellow), John Wiley & Sons, New York, **1991**, pp. 115–175.
- [71] L. M. Steinberg, J. M. Regan, *Appl. Environ. Microbiol.* **2008**, *74*, 6663–6671.
- [72] C. Koch, D. Popiel, F. Harnisch, *ChemElectroChem* **2014**, *1*, 1923–1931.
- [73] C. Koch, A. Kuchenbuch, J. Kretzschmar, H. Wedwitschka, J. Liebetrau, S. Müller, F. Harnisch, *RSC Adv.* **2015**, *5*, 31329–31340.

Manuscript received: November 9, 2020
Revised manuscript received: December 28, 2020
Accepted manuscript online: January 2, 2021
Version of record online: January 19, 2021